

Article

Plasma Temperatures in the Martian Subsolar Magnetosheath: MAVEN Observations

Nian Ren , Chao Shen * and Yong Ji 

School of Science, Harbin Institute of Technology, Shenzhen 518055, China

* Correspondence: shenchao@hit.edu.cn

Abstract: We studied the thermal features of magnetized plasmas in the Martian subsolar magnetosheath using MAVEN's observations from 2014 to 2019. Statistical analyses show that the average ion and electron temperature in the Martian subsolar magnetosheath are 210 and 31 eV, respectively, which are significantly lower than their counterparts in the subsolar magnetosheaths of Earth and Saturn which both have an inherent magnetosphere. However, the ratio \bar{T}_i/\bar{T}_e in the Martian subsolar magnetosheath is about 6.8, which is very close to that of Earth and Saturn. We further investigated the relationship between T_i/T_e and the bulk ion flow velocity V_i , as well as the relationship between the total plasma beta β and V_i . Results show that the average value of T_i/T_e when $V_i < 300$ km/s is considerably higher than when $V_i > 300$ km/s. A value of V_i closer to 250–300 km/s leads to a higher average value of the total plasma beta β . These results confirm the prediction of previous researchers, that there is not enough room for solar wind thermalization as the distance between the Martian bow shock and the so-called obstacle is of the order of a solar wind proton gyroradius.

Keywords: Mars; plasma temperature; subsolar magnetosheath; thermalization



Citation: Ren, N.; Shen, C.; Ji, Y. Plasma Temperatures in the Martian Subsolar Magnetosheath: MAVEN Observations. *Magnetochemistry* **2022**, *8*, 88. <https://doi.org/10.3390/magnetochemistry8080088>

Academic Editor: Pankaj Attri

Received: 9 July 2022

Accepted: 8 August 2022

Published: 9 August 2022

Publisher's Note: MDPI stays neutral with regard to jurisdictional claims in published maps and institutional affiliations.



Copyright: © 2022 by the authors. Licensee MDPI, Basel, Switzerland. This article is an open access article distributed under the terms and conditions of the Creative Commons Attribution (CC BY) license (<https://creativecommons.org/licenses/by/4.0/>).

1. Introduction

Despite the fact that Mars lacks a global intrinsic magnetic field besides crustal magnetization [1], the Mars–solar wind interaction exhibits numerous features in common with those arising from the solar wind interacting with Earth, which has an intrinsic magnetic field. Observations indicate the presence of bow shock (BS), upstream foreshock, magnetosheath (MS), and an inner magnetosphere and magnetotail on Mars [2–5], similar to Earth. At the interface between unmagnetized Mars and the solar wind, the dynamic pressure of the solar wind balanced with the Lorentz force generated by the induced current and magnetic fields that are caused by ionospheric currents. The formations of the BS and MS are similar to the traditional magnetosphere.

Although the BS and MS belonging to planets in the solar system play similar roles, the BS and MS of Mars differ compared to other planets due to its small size. For Earth and Venus, the thicknesses of the BS and MS are significantly larger than the solar wind ion cyclotron scale, whereas Mars' BS and MS are comparable with the gyroradius of the protons. Moses et al. [6] recognized that solar wind thermalization is confined due to the small scale of the Martian MS. Dubinin et al. [7] indicated that the thermalization of protons from the solar wind and planetary ionosphere would extend from the BS into the induced magnetosphere.

Turbulent cascade existing in Alfvénic fluctuations is identified as the primary heating mechanism for charged particles in the solar wind. Based on the theoretical Kolmogorov $-5/3$ spectrum and Kraichnan $-3/2$ spectrum, Vasquez et al. [8] used magnetic field measurements by ACE spacecraft to evaluate the turbulent energy cascade rates and compared them with the same rate calculated by proton temperature and solar wind speed. The results showed that the turbulence in the solar wind is closer to Kraichnan turbulence. Moreover, Qudsi et al. [9] analyzed Parker Solar Probe data at 1 au and found that a

good correlation between the solar wind proton temperature and intermittent small-scale magnetic field coherent structures existed, which revealed the heating mechanism in detail. In addition, the kinetic microinstabilities associated with the parallel proton beta induce turbulence in space plasma and impose a constraint on ion temperature anisotropy [10].

The scientific exploration of the Martian MS started with Mariner-4 and the early Soviet Mars missions and was followed by Phobos-2, Mars Global Surveyor (MGS), and Mars Express (MEX). Early Soviet Mars missions (the Mars-2, 3, and 5 missions) discovered the BS and MS for Mars [11]. By examining plasma and magnetic field data from Phobos-2, Dubinin et al. [12] discovered that the Martian MS is filled with intense bi-ion magnetoacoustic waves, which may evolve to multiple shock-like structures. Furthermore, from measurements made by Phobos-2, Dubinin et al. [13] revealed that the interplanetary magnetic field (IMF) controlled the asymmetry of the BS and MS. MGS further deepens our understanding of the dynamic physics of the MS. Based on observations consisting of 282 MS crossings, Bertucci et al. [5] reported that linearly polarized ultra-low frequency fluctuations of the magnetic field and superthermal electron detected in the Martian MS occupied at least 48% of the entire observation time. These compressive magnetic field oscillations were found to be anticorrelated with the superthermal electron density, implying that they are mirror mode waves [14]. MEX supplied further observational details to explore how thermal pressure in the MS balances solar wind dynamic pressure on the upstream side and magnetic pressure from the field piled up on the downstream side [15].

The Mars Atmosphere and Volatile Evolution (MAVEN) mission [16], initiated in 2013, is equipped with advanced instruments and has diverse orbits, providing high-quality data to study the Mars–solar wind interaction. To date, MAVEN’s observations have broadened the understanding of the distribution and role of electromagnetic waves in the Martian MS (including Alfvén waves) [17], the prevalence of wave power in multiple frequency bands [18], and plasma heating caused by these waves [19]. These results indicate the presence of nonthermal plasma and associated plasma instabilities in the Martian MS, reinforcing the hypothesis that the Martian MS is not sufficiently large to allow full thermalization of the shocked solar wind plasma, as predicted by Moses et al. [6].

Researchers studied the position of the Martian MS in detail. Slavin and Holzer [20] conducted a preliminary study of the position and shape of the BS of Mars using data from the “Mars” series of spacecraft. Trotignon et al. [21] determined the position of the Martian BS from 120 BS crossings based on data from Phobos 2. They argued that the position of the BS of Mars depends on solar activity. In contrast, the subsolar stand-off distance appears to vary slightly with the solar wind dynamic pressure. Since the arrival of the MGS, more extensive research has been carried out on the shape and structure of the magnetic pileup boundary (MPB) and the BS of Mars. Vignes et al. [22] published results on the location and shape of the BS and MPB reconstructed from 450 BS and 488 MPB crossings detected by the MAG/ER instrument during the first year of the MGS mission. Owing to the larger number of crossings, the results are more accurate.

In addition to the results of Vignes et al. [22], other researchers adopted the same method as Vignes et al. to determine the shape of the boundaries of Mars. Trotignon et al. [23] obtained the shape of the BS and the MPB from the fusion of Phobos 2 and MGS data. Edberg et al. [24] determined the location of the MPB and the BS by identifying MPB and BS crossings from the entire MAG/ER dataset from the premapping phase of the MGS mission.

In a previous study, the quantitative relationship between the temperature of the steady solar corona and that of the planetary MSs was derived [25]. This indicates that average plasma temperatures at the subsolar MSs of the planets with inherent magnetospheres are all close to the mean temperature of the corona. Systematic statistical analyses found that the average proton/ion temperatures at the subsolar MSs of Mercury, Earth, Jupiter, and Saturn are 414, 325, 309, and 304 eV, respectively, whereas the same average electron temperatures for Earth and Saturn are 47 and 37 eV, respectively (no electron data are available for Mercury and Jupiter at present). The average plasma temperatures of the subsolar MSs of Earth and Saturn are 184 and 171 eV, respectively. Statistical analyses for

the plasma temperatures at the subsolar MSs of planets with inherent magnetospheres (Mercury, Earth, Jupiter, and Saturn) confirmed these theoretical estimations. However, the exact thermal properties of the subsolar MS of Mars remain unclear and must be investigated in detail.

In this study, we make full use of MAVEN's unique capabilities to study the plasma temperatures in the Martian subsolar MS. Statistical analyses show that the average ion and electron temperatures in the Martian subsolar MS are 210 and 31 eV, respectively, which are significantly lower than their counterparts in the subsolar magnetosheaths of Earth and Saturn.

2. Instruments and Data

The solar wind ion analyzer (SWIA) [26,27] onboard MAVEN acquires measurements of solar wind ions both in the undisturbed upstream solar wind and in the post-shock MS. SWIA utilizes a toroidal energy analyzer with electrostatic deflectors to provide a broad $360^\circ \times 90^\circ$ field of view on a three-axis spacecraft, with a mechanical attenuator to enable a broad dynamic range. SWIA provides high cadence measurements of ion velocity distributions with high energy resolution (14.5%) and angular resolution ($3.75^\circ \times 4.5^\circ$ in the sunward direction, $22.5^\circ \times 22.5^\circ$ elsewhere), and a broad energy range of 5 eV to 25 keV. According to the description of Halekas et al. [27], the SWIA instrument provides several different types of data, including coarse 3-D distributions, fine 3-D distributions, onboard-computed moments, and energy spectra. Coarse 3-D distributions cover the full SWIA angular and energy range with lower resolutions, while fine 3-D distributions cover a limited range of phase space with high resolutions. Onboard-computed moments are computed onboard from coarse and fine 3-D ion distributions. In this study, we utilize onboard-computed moments to acquire the H^+ temperatures in the Martian MS.

The solar wind electron analyzer (SWEA) [28] is a symmetric hemispheric electrostatic analyzer with deflectors. It is well suited to measuring the energy and angular distributions of 3–4600 eV solar wind and MS electrons and ionospheric photoelectrons in the Mars environment. With these measurements, the instrument: (1) determines the electron impact ionization rates in all regions sampled by MAVEN, (2) distinguishes the energy spectra of ionospheric primary photoelectrons and the solar wind, MS, and magnetotail electrons to determine the plasma environment, (3) calculates electron pitch angle distributions to determine the topology of magnetic fields from both external and crustal sources, and (4) identifies auroral (~keV) electron populations and determines their role in ionization and dissociation processes. As described by Mitchell et al. [28], SWEA provides three data products: 3-D distributions, pitch angle distributions, and omnidirectional energy spectra. In this study, we calculate the electron temperatures in the Martian MS based on electron 3-D distribution after correcting for the spacecraft potential. Further, we plot the electron energy spectra according to omnidirectional energy spectra.

The magnetic field instrumentation onboard MAVEN contains two independent tri-axial fluxgate magnetometer sensors, located at the out end of the two solar arrays [29]. Each magnetometer measures the surrounding vector magnetic field over a wide range (up to 65,536 nT per axis) with the highest resolution of 0.008 nT and an accuracy of <0.05%. Both magnetometers sample the ambient magnetic field at an intrinsic sample rate of 32 vector samples per second. The magnetometers return magnetic field measurements in three coordinates: pc (planetocentric coordinates), pl (payload coordinates), and ss (Sun-state coordinates). In this study, we employ the magnetic field measurements in ss with a resolution of 1 s.

3. MAVEN Observations

In contrast to Earth's MS, whose scale is significantly larger than the mean gyroradius of solar wind ions, the MS of Mars has a thickness close to the gyroradius of ions in the solar wind. As a precondition to studying the plasma temperatures in the Martian subsolar MS, the location of the Martian MS must be determined. In this study, the model

proposed by Edberg et al. [24] is adopted to identify the Martian MS, as that model relies on more crossings and is more accurate than other empirical models [22,23]. The MS is located in the transition region between the BS and MPB. In the period from 2014 to 2019, we identified the time intervals when MAVEN was in the Martian subsolar MS ($\theta \leq 30^\circ$, $\theta = \arctan \frac{\sqrt{Y_{MSO}^2 + Z_{MSO}^2}}{X_{MSO}}$, MSO is the Mars solar orbital coordinate system) based on the model of Edberg et al. [24]. Notably, the model of Edberg et al. [24] provides only the average positions of the BS and MPB. However, due to the variation in the solar wind conditions and the IMF, the positions of the BS and MPB are variable. To ensure that MAVEN is located in the subsolar MS of Mars, we must determine the energy spectrum of electron flux and the magnetic field measurements. Figure 1 shows an example of Martian MS crossing observed by MAVEN. The time interval from 21:10:00 to 21:30:00 on 7 January 2017, is selected, during which MAVEN is located in the Martian subsolar MS ($\theta \leq 30^\circ$). The upper panel of Figure 1 shows the energy spectrum of the electron flux, and the lower panel displays the total magnetic field intensity (Bt) in the MSO coordinate system. After 21:22:56 UT (the black dotted line), the electron energy spectrum and the Bt change simultaneously and significantly. Before 21:22:56 UT, the electron flux with energy ~ 100 eV can reach as high as 10^9 ($\text{eV}/\text{cm}^2 \text{ sec ster eV}$), after which the electron flux drops rapidly by two orders of magnitude to $\sim 10^7$ ($\text{eV}/\text{cm}^2 \text{ sec ster eV}$). Before 21:22:56 UT, Bt is very high and fluctuates dramatically between 20 and 40 nT. After 21:22:56 UT, Bt drops rapidly to below 10 nT and fluctuates slightly. Both the change in electron energy flux and the variation in the Bt indicate that MAVEN was passing from the Martian MS to the solar wind. Therefore, we identify that MAVEN is truly located in the subsolar MS of Mars from 21:10:00 to 21:22:56 on 7 January 2017. Throughout all time intervals, we found 1219 intervals in which MAVEN was located in the subsolar MS of Mars by identifying similar variations in the electron energy flux and Bt as shown in Figure 1.

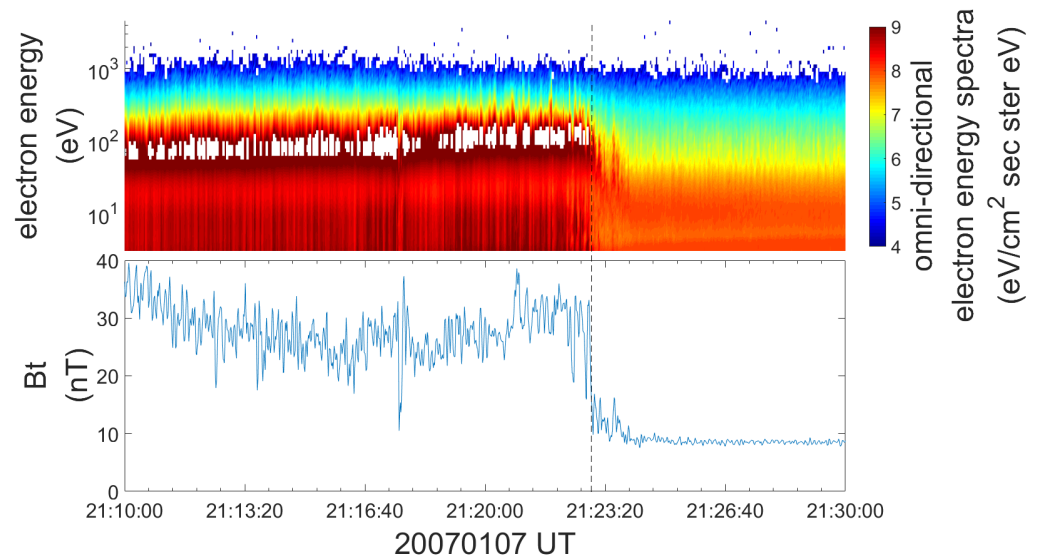


Figure 1. Electron energy flux spectrum and the total magnetic field for MAVEN passing from the Martian MS to the solar wind.

Based on the selected data belonging to 1219 time intervals, we performed statistical analysis and obtained the distribution of plasma temperatures in the subsolar MS of Mars. For the ion temperatures, we utilized onboard-computed moments provided by the SWIA onboard MAVEN to determine the magnitudes. The ion temperatures are approximate to proton temperatures, as protons are absolutely the dominant components of the solar wind. In the statistical analysis, we collected one data point from every minute. The statistical distribution of ion temperatures in the Martian subsolar MS is illustrated in Figure 2. The maximum ion temperature in the MS of Mars can reach 800 eV. The average ion temperature is $\bar{T}_i \approx 210$ eV, and the most probable ion temperature is $T_{\text{imp}} \approx 165$ eV, with

a standard deviation of $S_{T_i} \approx 101$ eV. Furthermore, we obtained electron temperatures in the Martian subsolar MS based on electron 3-D distributions after correcting the spacecraft potential. Electron 3-D distribution is one of the data products supplied by the SWEA onboard MAVEN. As for ion temperatures, we collected one data point from every minute for electron temperatures. The statistical distribution of electron temperatures in the Martian subsolar MS is shown in Figure 3. The maximum electron temperature in the Martian subsolar MS can reach 90 eV. The average electron temperature is $\bar{T}_e \approx 31$ eV, and the most probable electron temperature is $T_{emp} \approx 29$ eV, with a standard deviation of $S_{T_e} \approx 11$ eV. Therefore, the average plasma temperature in the Martian subsolar MS is $\bar{T} = \frac{1}{2}(\bar{T}_i + \bar{T}_e) = \frac{1}{2}(210 + 31) \approx 121$ eV. Wang et al. [30] used THEMIS measurements to determine the distributions of ion and electron temperatures in the Earth's MS. The result indicates that the average ion temperature in the Earth's subsolar MS is larger than 300 eV, while the average electron temperature is larger than 40 eV. Thomsen et al. [31] used the dataset from Cassini to determine the distributions of ion and electron temperatures in Saturn's MS. The result shows that the average ion temperature in Saturn's subsolar MS is larger than 300 eV, and the average electron temperature is ~ 40 eV. The study by Shen et al. [25] indicates that the average plasma temperatures in the subsolar MS of Earth and Saturn are 184 and 171 eV, respectively. Evidently, the average plasma temperature in the Martian subsolar MS is smaller than those on Earth and Saturn. However, the ratio of the ion to electron temperature in the Martian subsolar MS is approximately seven, which is nearly the same as that of the Earth's and Saturn's subsolar MSs [25,30,31].

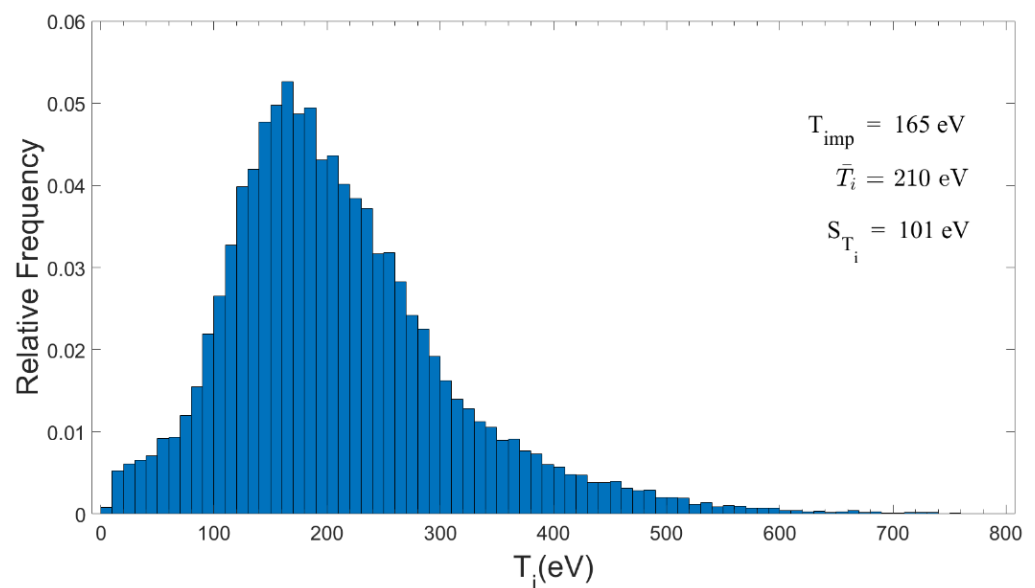


Figure 2. Ion temperature distribution in the subsolar region of the Martian MS based on data selected from SWIA onboard MAVEN from 2014 to 2019.

In addition to the plasma temperatures, we counted the bulk ion flow velocity and the total plasma beta (the ratio of total plasma thermal pressure to plasma magnetic pressure) in the Martian subsolar MS, which are important parameters of MS plasmas. Figures 4 and 5 show the statistical results. The maximum bulk ion flow velocity in Martian subsolar MS can reach 600 km/s (Figure 4). The average bulk ion flow velocity is $\bar{V}_i = 138$ km/s, and the most probable bulk ion flow velocity is $V_{imp} = 107.5$ km/s, with a standard deviation of $S_{V_i} = 77$ km/s. As shown in Figure 5, the maximum total plasma beta β in the Martian subsolar MS can reach 60. The average total plasma beta is $\bar{\beta} = 5.4$, and the most probable total plasma beta is $\beta_{mp} = 1.75$, with a standard deviation of $S_{\beta} = 7.3$.

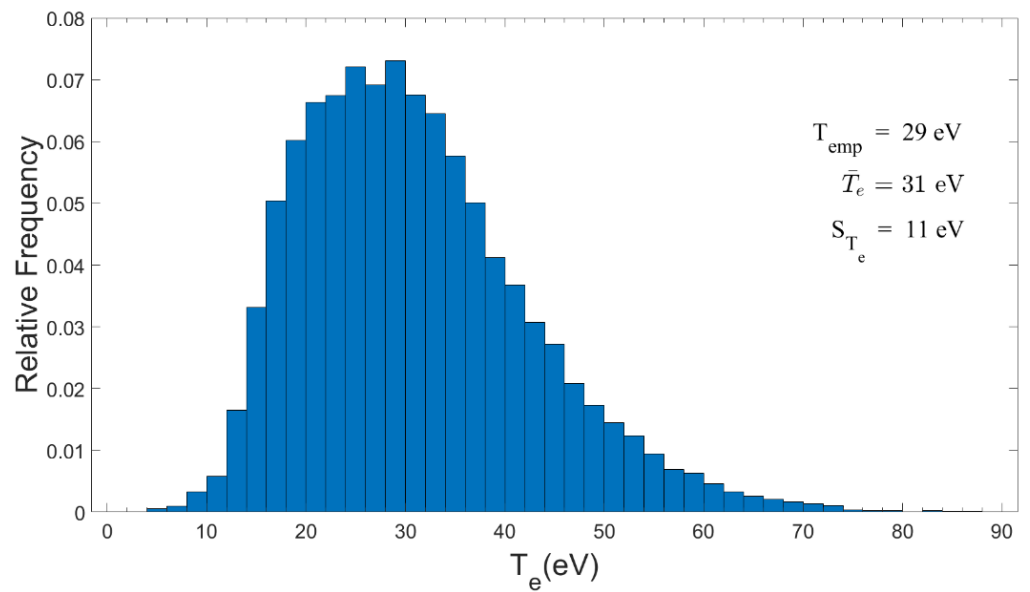


Figure 3. Electron temperature distribution in the subsolar region of the Martian MS based on data selected from SWEA onboard MAVEN from 2014 to 2019.

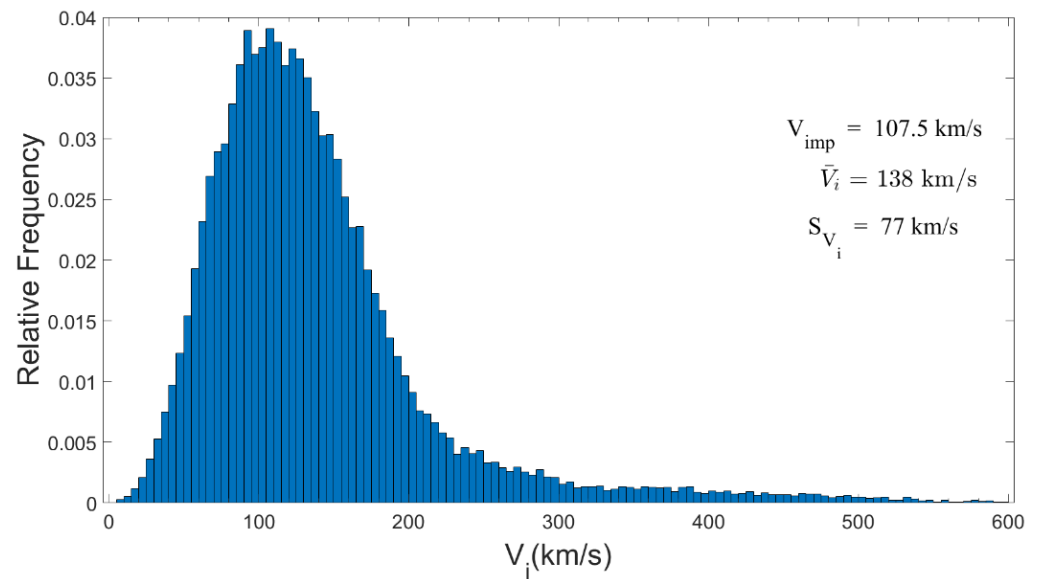


Figure 4. Bulk ion flow velocity distribution in the subsolar region of the Martian MS based on data selected from SWIA onboard MAVEN from 2014 to 2019.

Furthermore, the relationship between T_i/T_e and the bulk ion flow velocity V_i , as well as the relationship between the total plasma beta and V_i were also investigated. Figure 6 shows that the distribution of data points in the $T_i/T_e - V_i$ plane presents two distinct characteristics: most points fall in the region where T_i/T_e is larger than three and less than 15, and V_i is below 300 km/s, while the remaining points are located in the region where T_i/T_e is mostly below five, and V_i is over 300 km/s. The result indicates that the distribution of T_i/T_e depends on the bulk ion flow velocity V_i . Figure 7 shows a more precise result. The average values of T_i/T_e vary between seven and nine when $V_i < 300$ km/s. In contrast, the average values of T_i/T_e vary between two and five when $V_i > 300$ km/s, and are significantly lower than when $V_i < 300$ km/s. To reveal how V_i affects the magnitude of T_i/T_e , we investigated the variation of T_i and T_e with V_i . As shown in Figure 8, the average values of T_i are larger than 200 eV, and the maximum value can reach 275 eV when $V_i < 300$ km/s. In contrast, the average values of T_i are

smaller than 160 eV, and the minimum value is 89 eV when $V_i > 300$ km/s. These results indicate that compared to when $V_i < 300$ km/s, the ions are not sufficiently heated when $V_i > 300$ km/s. This can be attributed to the following: because the thickness of the Martian MS is comparable to the gyroradius of the protons, the higher-velocity ions ($V_i > 300$ km/s) enter the Martian ionosphere before they are fully heated. As shown in Figure 9, the average values of T_e exhibit a positive correlation with V_i for $V_i < 150$ km/s, and are invariant when $V_i > 150$ km/s. Combining Figures 8 and 9, we can conclude that the difference in the average values of T_i/T_e separated by $V_i = 300$ km/s is mainly due to insufficient thermalization of ions when $V_i > 300$ km/s. The fact that T_i is obviously larger than T_e is consistent with the turbulent cascade heating mechanism investigated. In terms of the cascade picture, the energy originates from a large scale and transfers to a small scale, so that ions having a larger gyration radius would receive cascade energy first and be accelerated compared to electrons that have a small gyration radius. This can explain why T_i is larger than T_e . Finally, we investigate the relationship between the total plasma beta and the bulk ion flow velocity V_i . As shown in Figure 10, when the bulk ion flow velocity V_i is between 250 and 300 km/s, the total plasma beta β reaches the maximum and drops on either side.

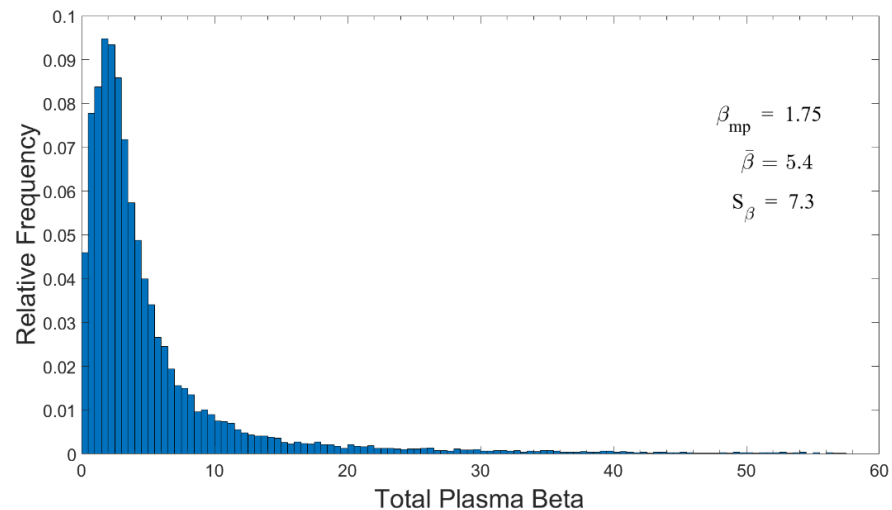


Figure 5. Total plasma beta distribution in the subsolar region of the Martian MS. Data were selected from SWIA, SWEA, and fluxgate magnetometer sensors onboard MAVEN from 2014 to 2019.

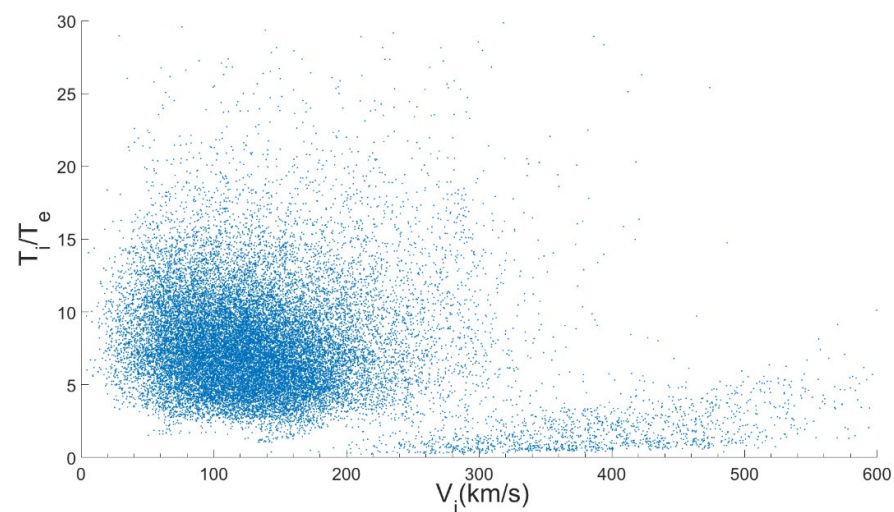


Figure 6. Scatter plot of T_i/T_e and V_i .

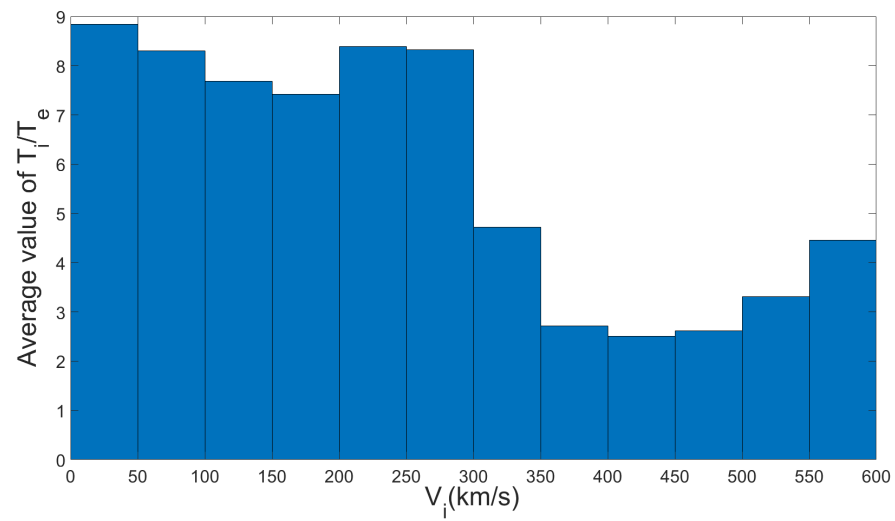


Figure 7. Relationship between average T_i/T_e and bulk ion flow velocity V_i .

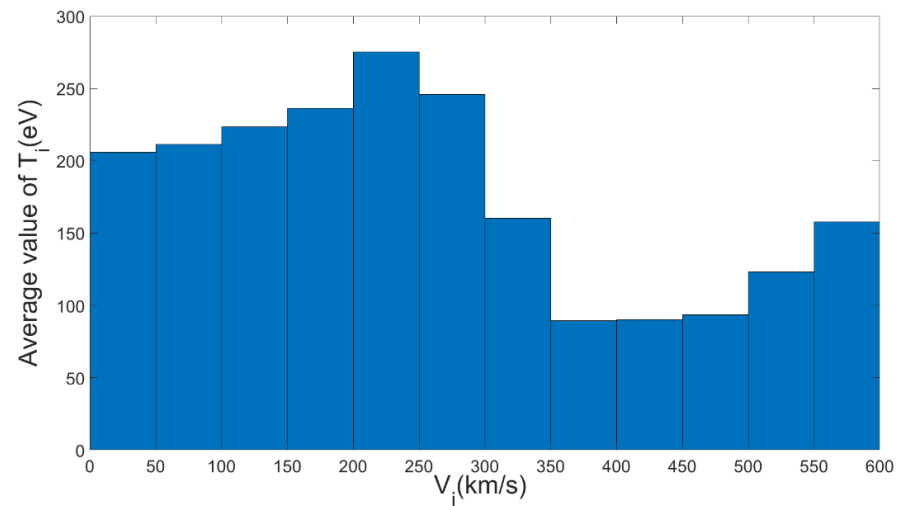


Figure 8. Relationship between average T_i and bulk ion flow velocity V_i .

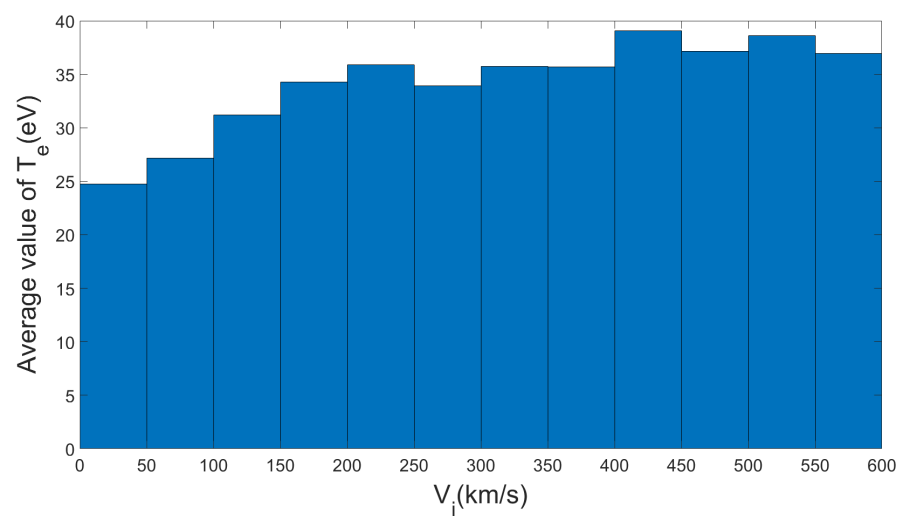


Figure 9. Relationship between average T_e and bulk ion flow velocity V_i .

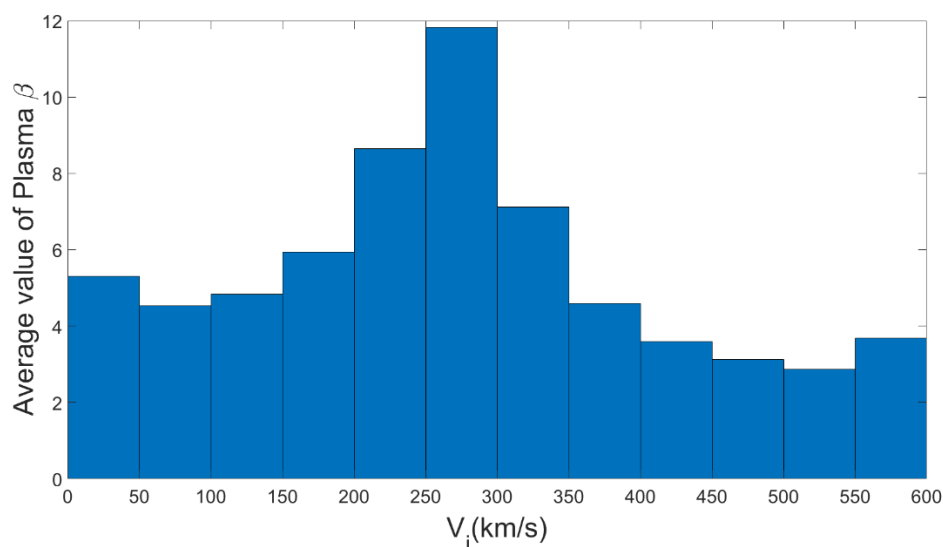


Figure 10. Relationship between the average total plasma beta β and bulk ion flow velocity V_i .

4. Discussion and Conclusions

The average ion and electron temperatures in the Martian subsolar MS are 210 and 31 eV, respectively, both values being lower than those on Earth and Saturn [25,30,31]. This observation indicates that the shocked solar wind plasma in the Martian subsolar MS is not fully heated. To confirm this hypothesis, we further investigated the bulk ion flow velocity in the Martian subsolar MS. As shown in Figure 4, the average bulk ion flow velocity in the Martian subsolar MS is $\bar{V}_i = 138$ km/s. In contrast, according to the observations of the Earth's MS [30] and Saturn's MS [31], the bulk ion flow velocity in the MS of these two planets is below 100 km/s, which is considerably smaller than that in the Martian subsolar MS. This means that a part of the kinetic energy of the plasma has not been converted into heat energy in the Martian MS before the plasma flows out of the MS. As the Martian MS has a comparable thickness to the gyroradius of the protons, the solar wind plasmas cannot be sufficiently decelerated and impact the ionosphere of Mars with considerable kinetic energy. The results of this study confirm the prediction of Moses et al. [6] that the solar wind is likely to thermalize incompletely before encountering the obstacle for typical solar wind conditions because of the small scale of the Martian MS. It is worth noting that the ratio \bar{T}_i/\bar{T}_e in the Martian subsolar MS is ~ 6.8 , which is very close to that of Earth and Saturn [25,30,31]. This suggests that the plasma heating mechanisms in the MS of Mars, Earth, and Saturn are similar.

The relationship of T_i/T_e and the total plasma beta β with the bulk ion flow velocity V_i was likewise studied. The results indicate that the average value of T_i/T_e when $V_i < 300$ km/s is significantly higher than when $V_i > 300$ km/s. By analyzing the relationship between ion temperatures T_i and V_i , as well as the relationship between electron temperatures T_e and V_i , we found that the reason for the difference in the average value of T_i/T_e is mainly due to the ions not being sufficiently heated when $V_i < 300$ km/s. Furthermore, when V_i is 250–300 km/s, the average total plasma beta β reaches its maximum, which indicates the most efficient energy transformation from the solar wind kinetic energy to internal energy.

Author Contributions: Conceptualization, N.R. and C.S.; methodology, N.R.; software, N.R.; validation, N.R.; formal analysis, N.R. and C.S.; investigation, N.R., C.S. and Y.J.; resources, N.R.; data curation, N.R.; writing—original draft preparation, N.R.; writing—review and editing, N.R., C.S. and Y.J.; visualization, N.R.; supervision, C.S.; project administration, C.S.; funding acquisition, C.S. All authors have read and agreed to the published version of the manuscript.

Funding: This work was supported by National Natural Science Foundation of China (Grant No. 42130202 and 41874190) and the Shenzhen Technology Project (JCYJ20190806144013077).

Institutional Review Board Statement: Not applicable.

Informed Consent Statement: Not applicable.

Data Availability Statement: All MAVEN data are available on the Planetary Data System <https://pds.nasa.gov> (accessed on 28 July 2021).

Acknowledgments: We acknowledge the MAVEN SWIA, SWEA, and MAG teams for providing these high-quality data.

Conflicts of Interest: The authors declare no conflict of interest.

References

1. Acuña, M.H.; Connerney, J.E.P.; Wasilewski, P.; Lin, R.P.; Anderson, K.A.; Carlson, C.W.; Mcfadden, J.; Curtis, D.W.; Reme, H.; Cros, A.; et al. Mars Observer magnetic fields investigation. *J. Geophys. Res. Planets* **1992**, *97*, 7799–7814. [[CrossRef](#)]
2. Nagy, A.F.; Winterhalter, D.; Sauer, K.; Cravens, T.E.; Brecht, S.; Mazelle, C.; Crider, D.; Kallio, E.; Zakharov, A.; Dubinin, E.; et al. The plasma environment of Mars. *Space Sci. Rev.* **2004**, *111*, 33–114. [[CrossRef](#)]
3. Mazelle, C.; Winterhalter, D.; Sauer, K.; Trotignon, J.G.; Acuna, M.H.; Baumgärtel, K.; Bertucci, C.; Brain, D.A.; Brecht, S.H.; Delva, M.; et al. Bow shock and upstream phenomena at Mars. *Space Sci. Rev.* **2004**, *111*, 115–181. [[CrossRef](#)]
4. Dubinin, E.; Fränz, M.; Woch, J.; Roussos, E.; Barabash, S.; Lundin, R.; Winningham, J.D.; Frahm, R.A.; Acuna, M. Plasma morphology at Mars. ASPERA-3 observations. *Space Sci. Rev.* **2006**, *126*, 209–238. [[CrossRef](#)]
5. Bertucci, C.; Duru, F.; Edberg, N.; Fraenz, M.; Martinecz, C.; Szego, K.; Vaisberg, O. The induced magnetospheres of Mars, Venus, and Titan. *Space Sci. Rev.* **2011**, *162*, 113–171. [[CrossRef](#)]
6. Moses, S.L.; Coroniti, F.V.; Scarf, F.L. Expectations for the microphysics of the Mars-solar wind interaction. *Geophys. Res. Lett.* **1988**, *15*, 429–432. [[CrossRef](#)]
7. Dubinin, E.; Lundin, R.; Koskinen, H.; Norberg, O. Cold ions at the Martian bow shock: Phobos observations. *J. Geophys. Res. Space Phys.* **1993**, *98*, 5617–5623. [[CrossRef](#)]
8. Vasquez, B.J.; Smith, C.W.; Hamilton, K.; Macbride, B.T.; Leamon, R.J. Evaluation of the turbulent energy cascade rates from the upper inertial range in the solar wind at 1 au. *J. Geophys. Res. Space Phys.* **2007**, *112*, A07101. [[CrossRef](#)]
9. Qudsi, R.A.; Maruca, B.A.; Matthaeus, W.H.; Parashar, T.N.; Bandyopadhyay, R.; Chhiber, R.; Chasapis, A.; Goldstein, M.L.; Bale, S.D.; Bonnell, J.W.; et al. Observations of Heating along Intermittent Structures in the Inner Heliosphere from PSP Data. *Astrophys. J. Suppl. S.* **2020**, *246*, 46. [[CrossRef](#)]
10. Maruca, B.A.; Chasapis, A.; Gary, S.P.; Bandyopadhyay, R.; Chhiber, R.; Parashar, T.N.; Matthaeus, W.H.; Shay, M.A.; Burch, J.L.; Moore, T.E.; et al. MMS Observations of Beta-dependent Constraints on Ion Temperature Anisotropy in Earth's Magnetosheath. *Astrophys. J.* **2018**, *866*, 25. [[CrossRef](#)]
11. Vaisberg, O.L. The solar wind interaction with Mars: A review of results from previous Soviet missions to Mars. *Adv. Space Res.* **1992**, *12*, 137–161. [[CrossRef](#)]
12. Dubinin, E.M.; Sauer, K.; Baumgärtel, K.; Lundin, R. The Martian magnetosheath: PHOBOS-2 observations. *Adv. Space Res.* **1997**, *20*, 149–153. [[CrossRef](#)]
13. Dubinin, E.; Sauer, K.; Delva, M.; Tanaka, T. The IMF control of the Martian bow shock and plasma flow in the magnetosheath. Predictions of 3-D simulations and observations. *Earth Planets Space* **1998**, *50*, 873–882. [[CrossRef](#)]
14. Bertucci, C.; Mazelle, C.; Crider, D.H.; Mitchell, D.L.; Sauer, K.; Acuña, M.H.; Connerney, J.E.P.; Lin, R.P.; Ness, N.F.; Winterhalter, D. MGS MAG/ER observations at the magnetic pileup boundary of Mars: Draping enhancement and low frequency waves. *Adv. Space Res.* **2004**, *33*, 1938–1944. [[CrossRef](#)]
15. Dubinin, E.; Modolo, R.; Fraenz, M.; Woch, J.; Duru, F.; Akalin, F.; Gurnett, D.; Lundin, R.; Barabash, S.; Plaut, J.J.; et al. Structure and dynamics of the solar wind/ionosphere interface on Mars: MEX-ASPERA-3 and MEX-MARSIS observations. *Planet Space Sci.* **2008**, *35*, L11103. [[CrossRef](#)]
16. Jakosky, B.M.; Lin, R.P.; Grebowsky, J.M.; Luhmann, J.G.; Mitchell, D.F.; Beutelschies, G.; Priser, T.; Acuna, M.; Andersson, L.; Baird, D. The Mars atmosphere and volatile evolution (MAVEN) mission. *Space Sci. Rev.* **2015**, *195*, 3–48. [[CrossRef](#)]
17. Ruhunusiri, S.; Halekas, J.S.; Connerney, J.E.P.; Espley, J.R.; McFadden, J.P.; Larson, D.E.; Mitchell, D.L.; Mazelle, C.; Jakosky, B.M. Low-frequency waves in the Martian magnetosphere and their response to upstream solar wind driving conditions. *Geophys. Res. Lett.* **2015**, *42*, 8917–8924. [[CrossRef](#)]
18. Fowler, C.M.; Andersson, L.; Halekas, J.; Espley, J.R.; Mazelle, C.; Coughlin, E.R.; Ergun, R.E.; Andrews, D.J.; Connerney, J.E.P.; Jakosky, B. Electric and magnetic variations in the near Mars environment. *J. Geophys. Res. Space Phys.* **2017**, *122*, 8536–8559. [[CrossRef](#)]
19. Ruhunusiri, S.; Halekas, J.S.; Espley, J.R.; Mazelle, C.; Brain, D.; Harada, Y.; DiBraccio, G.A.; Livi, R.; Larson, D.E.; Mitchell, D.L. Characterization of turbulence in the Mars plasma environment with MAVEN observations. *J. Geophys. Res. Space Phys.* **2017**, *122*, 656–674. [[CrossRef](#)]

20. Slavin, J.A.; Holzer, R.E. Solar wind flow about the terrestrial planets 1. Modeling bow shock position and shape. *J. Geophys. Res. Space Phys.* **1981**, *86*, 11401–11418. [[CrossRef](#)]
21. Trotignon, J.G.; Grard, R.; Skalsky, A. Position and shape of the Martian bow shock: The Phobos 2 plasma wave system observations. *Planet Space Sci.* **1993**, *41*, 189–198. [[CrossRef](#)]
22. Vignes, D.; Mazelle, C.; Rme, H.; Acuña, M.H.; Connerney, J.E.P.; Lin, R.P.; Mitchell, D.L.; Cloutier, P.; Crider, D.H.; Ness, N.F. The solar wind interaction with Mars: Locations and shapes of the bow shock and the magnetic pile-up boundary from the observations of the MAG/ER Experiment onboard Mars Global Surveyor. *Geophys. Res. Lett.* **2000**, *27*, 49–52. [[CrossRef](#)]
23. Trotignon, J.G.; Mazelle, C.; Bertucci, C.; Acuña, M.H. Martian shock and magnetic pile-up boundary positions and shapes determined from the Phobos 2 and Mars Global Surveyor data sets. *Planet Space Sci.* **2006**, *54*, 357–369. [[CrossRef](#)]
24. Edberg, N.J.T.; Lester, M.; Cowley, S.W.H.; Eriksson, A.I. Statistical analysis of the location of the Martian magnetic pileup boundary and bow shock and the influence of crustal magnetic fields. *J. Geophys. Res. Space Phys.* **2008**, *113*, A08206. [[CrossRef](#)]
25. Shen, C.; Ren, N.; Ma, Y.; Qureshi, M.N.S.; Guo, Y. Relationship between the Temperatures of Solar Corona and Planetary Magnetosheaths. *J. Geophys. Res. Space Phys.* **2022**. (submitted).
26. Halekas, J.S.; Taylor, E.R.; Dalton, G.; Johnson, G.; Curtis, D.W.; McFadden, J.P.; Mitchell, D.L.; Lin, R.P.; Jakosky, B.M. The solar wind ion analyzer for MAVEN. *Space Sci. Rev.* **2015**, *195*, 125–151. [[CrossRef](#)]
27. Halekas, J.S.; Ruhunusiri, S.; Harada, Y.; Collinson, G.; Mitchell, D.L.; Mazelle, C.; McFadden, J.P.; Connerney, J.E.P.; Espley, J.R.; Eparvier, F.; et al. Structure, dynamics, and seasonal variability of the Mars-solar wind interaction: MAVEN Solar Wind Ion Analyzer in-flight performance and science results. *J. Geophys. Res. Space Phys.* **2017**, *122*, 547–578. [[CrossRef](#)]
28. Mitchell, D.L.; Mazelle, C.; Sauvaud, J.A.; Thocaven, J.J.; Rouzaud, J.; Fedorov, A.; Rouger, P.; Toubanc, D.; Taylor, E.; Gordon, D.; et al. The MAVEN solar wind electron analyzer. *Space Sci. Rev.* **2016**, *200*, 495–528. [[CrossRef](#)]
29. Connerney, J.E.P.; Espley, J.; Lawton, P.; Murphy, S.; Odom, J.; Oliverson, R.; Sheppard, D. The MAVEN magnetic field investigation. *Space Sci. Rev.* **2015**, *195*, 257–291. [[CrossRef](#)]
30. Wang, C.P.; Gkioulidou, M.; Lyons, L.R.; Angelopoulos, V. Spatial distributions of the ion to electron temperature ratio in the magnetosheath and plasma sheet. *J. Geophys. Res.* **2012**, *117*, A08215. [[CrossRef](#)]
31. Thomsen, M.F.; Coates, A.J.; Jackman, C.M.; Sergis, N.; Jia, X.; Hansen, K.C. Survey of magnetosheath plasma properties at Saturn and inference of upstream flow conditions. *J. Geophys. Res. Space Phys.* **2018**, *123*, 2034–2053. [[CrossRef](#)]